Information Sciences 268 (2014) 53–64

Contents lists available at ScienceDirect

Information Sciences

journal homepage: www.elsevier.com/locate/ins

A finger-knuckle-print recognition algorithm using phase-based local block matching

Shoichiro Aoyama *, Koichi Ito *, Takafumi Aoki

Graduate School of Information Sciences, Tohoku University, 6-6-05, Aramaki Aza Aoba, Sendai 980-8579, Japan

ARTICLE INFO

Article history:
Available online 23 August 2013

Keywords:
Finger-knuckle-print
Biometric
Phase-only correlation
Local block matching

ABSTRACT

This paper proposes a Finger-Knuckle-Print (FKP) recognition algorithm using Band-Limited Phase-Only Correlation (BLPOC)-based local block matching. The phase information obtained from 2D Discrete Fourier Transform (DFT) of images contains important information of image representation. The phase-based image matching, especially BLPOC-based image matching, is successfully applied to image recognition tasks for biometric recognition applications. To calculate the matching score, the proposed algorithm corrects the global and local deformation between FKP images using phase-based correspondence matching and the BLPOC-based local block matching, respectively. Experimental evaluation using the PolyU FKP database demonstrates the efficient recognition performance of the proposed algorithm compared with the state-of-the-art conventional algorithms.

© 2013 Elsevier Inc. All rights reserved.

1. Introduction

Biometric authentication has been receiving extensive attention with the need for robust human recognition techniques in various networked applications [1]. Biometric authentication (or simply biometrics) is to identify a person based on the physiological or behavioral characteristics such as fingerprint, face, iris, voice, and signature.

Among many biometric techniques, hand-based biometrics has been attracted lots of attention. Fingerprint [2], palmprint [3–6], hand geometry [7], Finger-Knuckle-Print (FKP) [8–22], and combinations of the above traits [23,24] have been used as biometric traits related to a hand. In this paper, we focus on recognizing a person using FKP patterns. An FKP is a pattern of outer finger knuckle surface which contains many fine ridge patterns and texture, and is expected to be one of the distinctive biometric traits.

So far, the FKP recognition algorithms have been proposed by many researchers as shown in Table 1. Woodard and Flynn [8] have proposed a curvature-based recognition algorithm using 3D finger surface taken by a 3D sensor, where this is the first attempt to use FKPs for biometric authentication. The use of the 3D sensor is not acceptable for the practical use due to its size, cost, weight, processing time, etc. On the other hand, the use of 2D FKP images makes it possible to realize compact and powerful biometric authentication systems. Ferrer et al. [9] have proposed a ridge feature-based algorithm which extracts ridge features from FKP images and evaluates their similarity using Hidden Markov Model (HMM) or Support Vector Machine (SVM). Kumar and Zhou have proposed a coding-based algorithm called KnuckleCode generated by using local Radon transform [12] and subspace-based algorithms such as Principal Component Analysis (PCA), Independent Component Analysis (ICA) and Linear Discriminant Analysis (LDA) [13]. Kumar [20] has proposed to use not only the finger knuckle pattern on the second joint, i.e., the metacarpophalangeal joint, but also the finger knuckle pattern on the first joint, i.e., the distal interphalangeal joint. Xiong et al. [15] have used Local Gabor Binary Patterns (LGBP) combining Gabor wavelet and

* Corresponding authors. Tel.: +81 22 795 7169; fax: +81 22 263 9308.
E-mail addresses: aoyama@aoki.ecei.tohoku.ac.jp (S. Aoyama), ito@aoki.ecei.tohoku.ac.jp (K. Ito), aoki@ecei.tohoku.ac.jp (T. Aoki).

0020-0255/$ - see front matter © 2013 Elsevier Inc. All rights reserved.
http://dx.doi.org/10.1016/j.ins.2013.08.025

Table 1
Summary of conventional FKP recognition algorithms.

Author	Trait	Feature	Similarity
Woodard and Flynn [8]	3D knuckle	Surface curvature	NCC
Ferrer et al. [9]	FKP	Ridge	HMM or SVM
Kumar and Zhou [12]	FKP	Localized Radon transform	Distance
Kumar and Ravikanth [13]	FKP	texture	PCA, ICA and LDA
Kumar [20]	Major and minor knuckle	LBP, Log-Gabor	Distance
Xiong et al. [15]	FKP	Local Gabor binary patterns	Distance
Morales et al. [16]	FKP	Gabor filter and SIFT	Distance
Zhang et al. [10]	FKP	Competitive code	Distance
Zhang et al. [11]	FKP	BLPOC	Correlation
Zhang et al. [14]	FKP	Improved competitive code and magnitude code	Distance
Zhang et al. [17]	FKP	Competitive code and BLPOC	Distance
Zhang et al. [18]	FKP	Phase congruency and BLPOC	Distance
Zhang and Li [22]	FKP	RCode1 and RCode2	Distance
Zichao et al. [19]	FKP	Orientation	Distance
Mittal et al. [21]	FKP	DAISY	Distance
Michael et al. [23]	Palmprint and FKP	Directional code	Distance
Zhu and Zhang [24]	Finger geometry, palmprint and FKP	Gradient	Correlation

Local Binary Patterns (LBPs) which are successfully applied to face recognition. Morales et al. [16] have used Orientation Enhanced Scale Invariant Feature Transform (OE-SIFT) which applies a Gabor filter to enhance the FKP images and perform SIFT-based matching to evaluate the similarity. Zhang et al. have proposed some FKP recognition algorithms using the competitive code generated by using Gabor filter bank [10], Band-Limited Phase-Only Correlation (BLPOC) [11], a combination method of improved competitive code and magnitude code [14], a combination method of competitive code and BLPOC [17], a combination method of phase congruency and BLPOC [18], and the Riesz transform based coding scheme [22]. Zichao et al. [19] have proposed a feature extraction method using steerable filters which can extract local orientation from FKP images. Mittal et al. [21] have proposed an FKP recognition algorithm using DAISY [25] which is one of the famous feature descriptors. In addition, the multi-modal hand-based recognition algorithms have been proposed [23,24]. Michael et al. [23] have developed a hand recognition system using palmprint and FKP, while Zhu and Zhang [24] have used finger geometry, palmprint and FKP. The recognition performance of the conventional FKP recognition algorithms may be degraded for FKP images having nonlinear deformation due to the movement of a finger, since these algorithms consider only rigid body transformation of FKP images.

In this paper, we propose an FKP recognition algorithm using BLPOC-based local block matching. POC is an image matching technique using the phase components in 2D Discrete Fourier Transforms (2D DFTs) of given images [26,27]. BLPOC is a modified version of POC which is dedicated to evaluate similarity between images [28] and has been used in various biometric recognition algorithms [29,30,11]. Most of POC-based biometric recognition algorithms cannot handle the nonlinear deformation of images, since the phase information obtained from the entire image is employed. In order to handle the nonlinear deformation of FKP images, the proposed algorithm employs local block matching using BLPOC, since the nonlinear deformation is approximately represented by the minute translational displacement between local image blocks. First, we correct the global transformation between FKP images which is estimated using phase-based correspondence matching. Next, we correct the minute translational displacement between each local image block pair using the BLPOC-based local block matching. Finally, we take the average of a set of the BLPOC functions calculated from each local image block pair and obtain the correlation peak value of the average BLPOC function as a matching score between the FKP images. Experimental evaluation using the PolyU FKP database [31] demonstrates efficient recognition performance of the proposed algorithm compared with the state-of-the-art conventional algorithms.

The rest of the paper is organized as follows: Section 2 describes the fundamentals of POC, BLPOC and phase-based correspondence matching. Section 3 describes FKP recognition algorithms using phase-based image matching and the proposed algorithm. Section 4 shows experiments for evaluating the performance of the proposed algorithm using the PolyU FKP database. Section 5 ends with some concluding remarks.

2. Phase-based image matching

This section describes the fundamentals of phase-based image matching, i.e., Phase-Only Correlation (POC), Band-Limited POC (BLPOC) and phase-based correspondence matching.

2.1. Phase-Only Correlation (POC)

We introduce the principle of a Phase-Only Correlation (POC) function (which is sometimes called the "phase-correlation function") [26,27].

Consider two $N_1 \times N_2$ images, $f(n_1, n_2)$ and $g(n_1, n_2)$, where we assume that the index ranges are $n_1 = -M_1,\ldots,M_1 (M_1 > 0)$ and $n_2 = -M_2,\ldots,M_2$ $(M_2 > 0)$ for mathematical simplicity, and hence $N_1 = 2M_1 + 1$ and $N_2 = 2M_2 + 1$. The discussion could be easily generalized to non-negative index ranges with power-of-two image size. Let $F(k_1, k_2)$ and $G(k_1, k_2)$ denote the 2D DFTs of $f(n_1, n_2)$ and $g(n_1, n_2)$, respectively. According to the definition of DFT [32], $F(k_1, k_2)$ and $G(k_1, k_2)$ are given by

$$F(k_1,k_2) = \sum_{n_1,n_2} f(n_1,n_2) W_{N_1}^{k_1 n_1} W_{N_2}^{k_2 n_2} = A_F(k_1,k_2) e^{j\theta_F(k_1,k_2)}, \tag{1}$$

$$G(k_1,k_2) = \sum_{n_1,n_2} g(n_1,n_2) W_{N_1}^{k_1 n_1} W_{N_2}^{k_2 n_2} = A_G(k_1,k_2) e^{j\theta_G(k_1,k_2)}, \tag{2}$$

respectively, where $k_1 = -M_1,\ldots,M_1$, $k_2 = -M_2,\ldots,M_2$, $W_{N_1} = e^{-j\frac{2\pi}{N_1}}$, $W_{N_2} = e^{-j\frac{2\pi}{N_2}}$, and $\sum_{n_1,n_2}$ denotes $\sum_{n_1=-M_1}^{M_1}\sum_{n_2=-M_2}^{M_2}$. $A_F(k_1, k_2)$ and $A_G(k_1, k_2)$ are amplitude, and $\theta_F(k_1, k_2)$ and $\theta_G(k_1, k_2)$ are phase. The normalized cross power spectrum $R_{FG}(k_1, k_2)$ is given by

$$R_{FG}(k_1,k_2) = \frac{F(k_1,k_2)\overline{G(k_1,k_2)}}{|F(k_1,k_2)\overline{G(k_1,k_2)}|} = e^{j\theta(k_1,k_2)}, \tag{3}$$

where $\overline{G(k_1,k_2)}$ is the complex conjugate of $G(k_1, k_2)$ and $\theta(k_1, k_2)$ denotes the phase difference $\theta_F(k_1, k_2) - \theta_G(k_1, k_2)$. The POC function $r_{fg}(n_1, n_2)$ is the 2D Inverse DFT (2D IDFT) of $R_{FG}(k_1, k_2)$ and is given by

$$r_{fg}(n_1,n_2) = \frac{1}{N_1 N_2} \sum_{k_1,k_2} R_{FG}(k_1,k_2) W_{N_1}^{-k_1 n_1} W_{N_2}^{-k_2 n_2}, \tag{4}$$

where $\sum_{k_1,k_2}$ denotes $\sum_{k_1=-M_1}^{M_1}\sum_{k_2=-M_2}^{M_2}$. When two images are similar, their POC function gives a distinct sharp peak. When two images are not similar, the peak drops significantly. The height of the peak gives a good similarity measure for image matching, and the location of the peak shows the translational displacement between the images.

We have proposed a high-accuracy translational displacement estimation method, which employs (i) an analytical function fitting technique to estimate the sub-pixel position of the correlation peak, (ii) a windowing technique to eliminate the effect of periodicity in 2D DFT, and (iii) a spectrum weighting technique to reduce the effect of aliasing and noise [27].

2.2. Band-Limited POC (BLPOC)

We have proposed a BLPOC (Band-Limited Phase-Only Correlation) function [28] dedicated to biometric recognition tasks. The idea to improve the matching performance is to eliminate meaningless high frequency components in the calculation of normalized cross power spectrum R_{FG} depending on the inherent frequency components of images. Assume that the ranges of the inherent frequency band are given by $k_1 = -K_1,\ldots,K_1$ and $k_2 = -K_2,\ldots,K_2$, where $0 \leqslant K_1 \leqslant M_1$ and $0 \leqslant K_2 \leqslant M_2$. Thus, the effective size of frequency spectrum is given by $L_1 = 2K_1 + 1$ and $L_2 = 2K_2 + 1$. The BLPOC function is given by

$$r_{fg}^{K_1 K_2}(n_1,n_2) = \frac{1}{L_1 L_2} {\sum_{k_1,k_2}}' R_{FG}(k_1,k_2) W_{L_1}^{-k_1 n_1} W_{L_2}^{-k_2 n_2}, \tag{5}$$

where $n_1 = -K_1,\ldots,K_1$, $n_2 = -K_2,\ldots,K_2$, and $\sum'_{k_1,k_2}$ denotes $\sum_{k_1=-K_1}^{K_1}\sum_{k_2=-K_2}^{K_2}$. Note that the maximum value of the correlation peak of the BLPOC function is always normalized to 1 and does not depend on L_1 and L_2.

2.3. Phase-based correspondence matching

In order to handle the nonlinear deformation of FKP images, we employ the sub-pixel correspondence matching using POC [33], which employs (i) a coarse-to-fine strategy using image pyramids for robust correspondence search and (ii) a sub-pixel translational displacement estimation method using POC for local block matching. Let $\boldsymbol{p}$ be a coordinate vector of a reference pixel in the reference image $I(n_1, n_2)$. The problem of sub-pixel correspondence search is to find a real-number coordinate vector $\boldsymbol{q}$ in the input image $J(n_1, n_2)$ that corresponds to the reference pixel $\boldsymbol{p}$ in $I(n_1, n_2)$. We briefly explain the procedure as follows.

Step 1: For $l = 1,2,\ldots,l_{\max}$, create the lth layer images $I_l(n_1, n_2)$ and $J_l(n_1, n_2)$, i.e., coarser versions of $I_0(n_1, n_2)$ $(= I(n_1, n_2))$ and $J_0(n_1, n_2)$ $(= J(n_1, n_2))$, recursively as follows:

$$I_l(n_1,n_2) = \frac{1}{4}\sum_{i_1=0}^{1}\sum_{i_2=0}^{1} I_{l-1}(2n_1+i_1, 2n_2+i_2), \tag{6}$$

$$J_l(n_1,n_2) = \frac{1}{4}\sum_{i_1=0}^{1}\sum_{i_2=0}^{1} J_{l-1}(2n_1+i_1, 2n_2+i_2). \tag{7}$$

Step 2: Estimate the displacement between $I_{l_{\max}}(n_1, n_2)$ and $J_{l_{\max}}(n_1, n_2)$ with pixel accuracy using POC-based image matching. Let the estimated displacement vector be $\boldsymbol{\delta}_{l_{\max}}$.
Step 3: For every layer $l = 1, 2, \ldots, l_{\max}$, calculate the coordinate $\boldsymbol{p}_l = (p_{l,1}, p_{l,2})$ corresponding to the original reference point $\boldsymbol{p}_0$ (= $\boldsymbol{p}$) recursively as follows:

$$\boldsymbol{p}_l = \left\lfloor \frac{1}{2}\boldsymbol{p}_{l-1} \right\rfloor = \left(\left\lfloor \frac{1}{2}p_{l-1,1} \right\rfloor, \left\lfloor \frac{1}{2}p_{l-1,2} \right\rfloor \right), \tag{8}$$

where $\lfloor z \rfloor$ denotes the operation to round the element of z to the nearest integer towards minus infinity.
Step 4: We assume that $\boldsymbol{q}_{l_{\max}} = \boldsymbol{p}_{l_{\max}} + \boldsymbol{\delta}_{l_{\max}}$ in the coarsest layer. Let $l = l_{\max} - 1$.
Step 5: From the lth layer images $I_l(n_1, n_2)$ and $J_l(n_1, n_2)$, extract two sub-images (or image blocks) $f_l(n_1, n_2)$ and $g_l(n_1, n_2)$ with their centers on $\boldsymbol{p}_l$ and $2\boldsymbol{q}_{l+1}$, respectively. The size of image blocks is $W_c \times W_c$ pixels.
Step 6: Estimate the displacement between $f_l(n_1, n_2)$ and $g_l(n_1, n_2)$ with pixel accuracy using POC-based image matching. Let the estimated displacement vector be $\boldsymbol{\delta}_l$. The lth layer correspondence $\boldsymbol{q}_l$ is determined as follows:

$$\boldsymbol{q}_l = 2\boldsymbol{q}_{l+1} + \boldsymbol{\delta}_l. \tag{9}$$

Step 7: Decrement the counter by 1 as $l \leftarrow l - 1$ and repeat from Step 5 to Step 7 while $l \geqslant 0$.
Step 8: From the original images $I_0(n_1, n_2)$ and $J_0(n_1, n_2)$, extract two image blocks with their centers on $\boldsymbol{p}_0$ and $\boldsymbol{q}_0$, respectively. Estimate the displacement between the two blocks with sub-pixel accuracy using POC-based image matching. Let the estimated displacement vector with sub-pixel accuracy be denoted by $\boldsymbol{\delta} = (\delta_1, \delta_2)$. Update the corresponding point as follows:

$$\boldsymbol{q} = \boldsymbol{q}_0 + \boldsymbol{\delta}. \tag{10}$$

The peak value of the POC function is also obtained as a measure of reliability in local block matching.

3. FKP recognition algorithms using phase-based image matching

This section presents the conventional POC-based FKP recognition algorithms: (A) the FKP recognition algorithm using BLPOC [11] and (B) the FKP recognition algorithm using phase-based correspondence matching [34]. Then, we describe (C) the FKP recognition algorithm using BLPOC-based local block matching which is proposed in this paper.

3.1. FKP recognition algorithm using BLPOC [11]

This algorithm is based on the global registration of FKP images using BLPOC.

The Region Of Interest (ROI) is extracted from the FKP image in the preprocessing. The translational displacement between the two ROI images is estimated using BLPOC and the two images are aligned according to the estimated displacement. Then, the common region of the two images is extracted. For example, Fig. 1(a) and (b) shows the registered and input FKP ROI images, and Fig. 1(c) and (d) shows their common regions. If the area ratio of the common region between the ROI images is below the threshold, the BLPOC function between the ROI images is calculated. Otherwise, the BLPOC function between the common regions is calculated. Finally, the highest peak value of the BLPOC function is obtained as the matching score between the two FKP images. Fig. 1(e) shows the BLPOC function between the FKP ROI images, while Fig. 1(f) shows the BLPOC function between the common regions. As a result, the use of the BLPOC function between common regions makes it possible to enhance the matching performance compared with the BLPOC function between the original images.

Local Global Information Combination (LGIC) [17] and LGIC_2 [18] have been proposed as the extended version of this algorithm. LGIC and LGIC_2 combine global and local similarities to calculate the matching score between ROI images. For both algorithms, the FKP recognition algorithm using BLPOC is employed to evaluate the global similarity between ROI images. To evaluate the local similarity between ROI images, LGIC employs CompCode, while LGIC_2 employs local phase and phase congruency. Both algorithms improve the performance of FKP recognition to combine the complementary information.

These algorithms consider only the global translational displacement between FKP images. Hence, the recognition performance of this algorithm is significantly dropped for FKP images having nonlinear deformation.

3.2. FKP recognition algorithm using phase-based correspondence matching [34]

This algorithm is based on the local registration of FKP images using phase-based correspondence matching which has been successfully applied to palmprint recognition algorithm [34].

The ROI image is extracted from the FKP image in the preprocessing. The 90 reference points are placed on the registered image and then the corresponding points on the input image are estimated using the phase-based correspondence matching as shown in Fig. 2(a) and (b). Then BLPOC functions between the local image blocks with their centers on corresponding point pairs are calculated. Finally, the matching score is calculated as the highest peak value of the average BLPOC function obtained from a set of BLPOC functions. To take the average of a set of BLPOC functions, the PNR (Peak-to-Noise Ratio) of the BLPOC function can be improved as shown in Fig. 2(c) and (d).

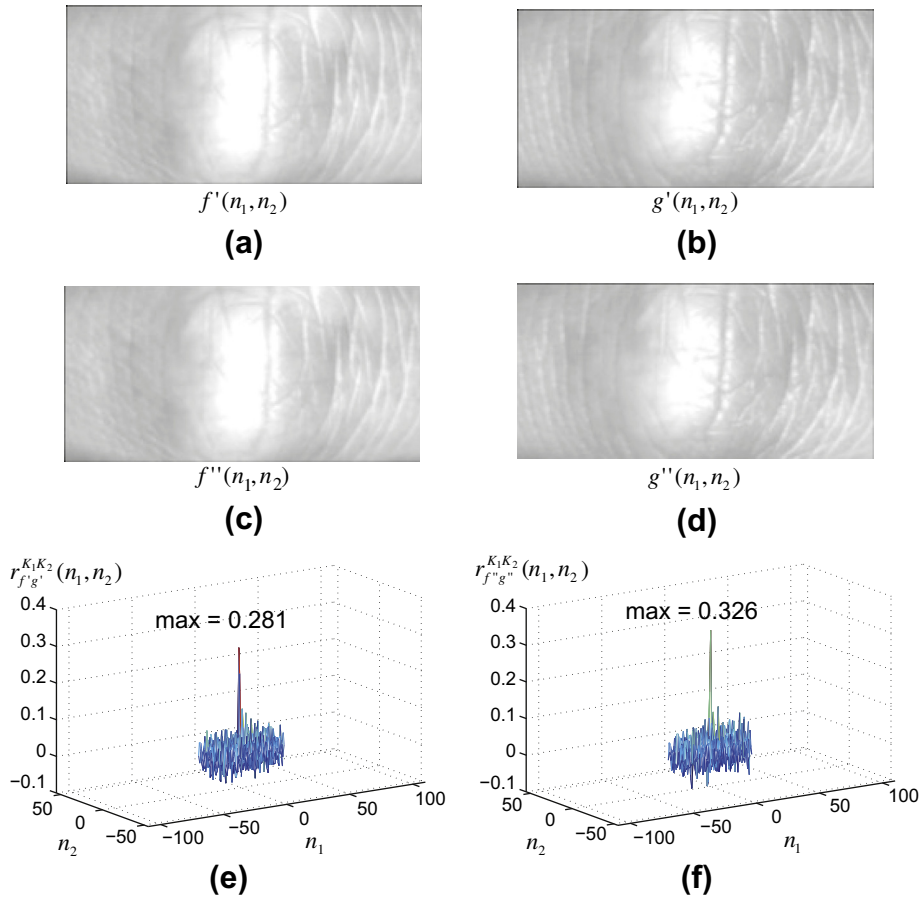

Fig. 1. Example of FKP recognition using BLPOC: (a) registered image, (b) input image, (c) common region of the registered image, (d) common region of the input image, (e) BLPOC function between FKP images (a) and (b), and (f) BLPOC function between common regions (c) and (d).

This algorithm can handle the nonlinear deformation of FKP images. However, the recognition performance of this algorithm may drop due to poor texture around the knuckle joint and the large movement of a finger, since the average BLPOC function is calculated from all the corresponding point pairs regardless of the reliability of correspondence.

3.3. Proposed FKP recognition algorithm

Sometimes, the FKP images include large deformation due to the movement of fingers. In order to handle the large deformation, the proposed algorithm employs global and local registration of FKP images using phase-based local block matching.

The ROI image is extracted from the FKP image in the preprocessing. The 90 reference points are placed on the registered image and the corresponding points on the input image are estimated using phase-based correspondence matching as shown in Fig. 3(a) and (b). To correct the global transformation between the images, we employ the affine transformation.

In the case of FKP images, the deformation is different between the left- and right-half regions of the knuckle joint. Hence, we estimate the parameters of the affine transformation for each region, and then normalize the affine transformation between the registered and input images. The parameters of the affine transformation are estimated using the reliable corresponding point pairs whose similarities, i.e., the peak value of the POC function, are above the threshold *th*. Let the reliable corresponding point pairs of the left-half region be $\boldsymbol{p}_L$ in the registered image and $\boldsymbol{q}_L$ in the input image, respectively, and let the reliable corresponding point pairs of the right-half region be $\boldsymbol{p}_R$ in the registered image and $\boldsymbol{q}_R$ in the input image, respectively as shown in Fig. 3(a) and (b). The transformation matrices between the corresponding point pairs for the left- and right-half regions are defined by

$$\boldsymbol{A}_L = \begin{bmatrix} a^L_{11} & a^L_{12} & a^L_{13} \\ a^L_{21} & a^L_{22} & a^L_{23} \\ 0 & 0 & 1 \end{bmatrix} \tag{11}$$

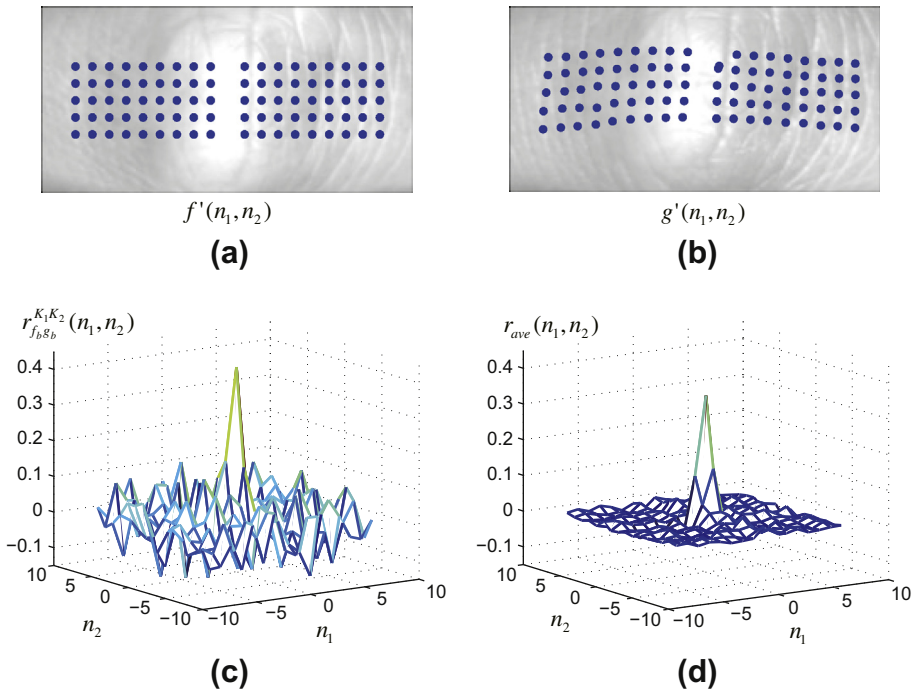

Fig. 2. Example of FKP recognition using phase-based correspondence matching: (a) reference points on the registered image, (b) corresponding points on the input image, (c) BLPOC function between a local image block pair, and (d) average BLPOC function.

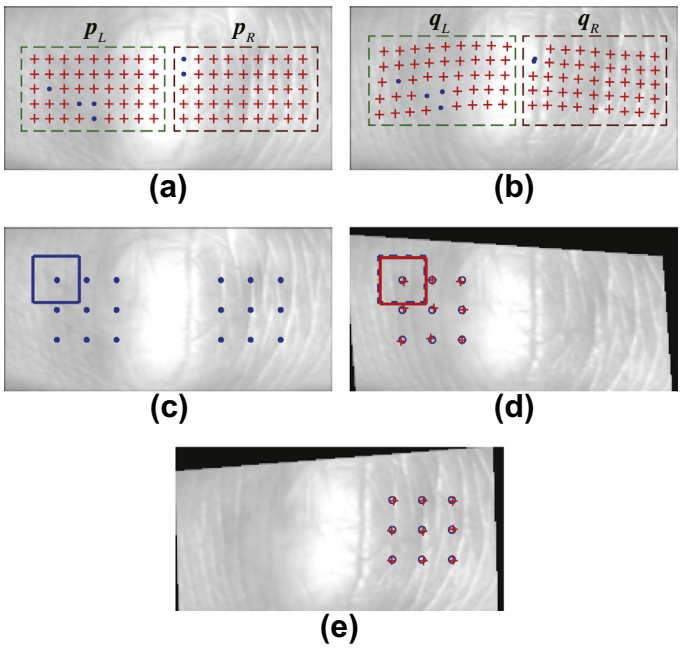

Fig. 3. Example of the proposed algorithm: (a) reference points on the registered image for global registration, (b) corresponding points on input image, where "+" in (a) and (b) indicates the reliable corresponding pairs whose similarities are above the threshold *th*, (c) reference points on the registered image for local registration and an example of a local image block, (d) the corresponding points on the left half of the input image after global registration with $\boldsymbol{A}_L$, and (e) the corresponding points on the right half of the input image after global registration with $\boldsymbol{A}_R$, where "○" and "+" in (d) and (e) indicate the corresponding points before and after local registration, respectively.

and

$$\boldsymbol{A}_R = \begin{bmatrix} a_{11}^R & a_{12}^R & a_{13}^R \\ a_{21}^R & a_{22}^R & a_{23}^R \\ 0 & 0 & 1 \end{bmatrix}, \tag{12}$$

respectively. The relation between the corresponding point pairs for the left- and right-half regions can be written as

$$\bar{\boldsymbol{q}}_L = \boldsymbol{A}_L \bar{\boldsymbol{p}}_L, \tag{13}$$

$$\bar{\boldsymbol{q}}_R = \boldsymbol{A}_R \bar{\boldsymbol{p}}_R, \tag{14}$$

respectively, where $\bar{z}$ indicates the homogeneous vector of z. The parameters of $\boldsymbol{A}_L$ and $\boldsymbol{A}_R$ are estimated by solving a set of linear simultaneous equations as the linear least-squares problem. We normalize the global deformation between the images using the estimated affine transformation matrices for each region. Fig. 3(d) and (e) shows the FKP images after global registration of left- and right-half regions, respectively.

Then, we calculate the matching score in consideration of nonlinear deformation. We assume that the nonlinear deformation is approximately represented by the minute translational displacement between local image blocks. First, the 18 local image blocks are extracted from the registered image as shown in Fig. 3(c). The 9 local image blocks on the left half of the image are for the left-half region of the FKP image, while the 9 blocks on the right half of the image are for the right-half region of the FKP image. The local block images of the input image are also extracted from the same position of the registered image. The translational displacement between each local image block pair is estimated using BLPOC, and then the local block images on the registered image are extracted in consideration of the estimated translational displacement as shown in Fig. 3(d). We calculate the BLPOC function between each local block image pair and take the average of a set of the BLPOC functions. Finally, the matching score between the FKP images is obtained as the highest peak value of the average BLPOC function.

As mentioned above, it is expected that the proposed algorithm is robust against the nonlinear deformation of FKP images compared with the conventional algorithms [11,17,18,34] described in Sections 3.1 and 3.2. Ref. [11] aligns only the global translational displacement between ROI images estimated by BLPOC. Refs. [17,18] also align only the global translational displacement estimated by BLPOC, and then calculate the matching score using the global and local similarities between ROI images. Ref. [34] considers the local translational displacement between local block images to calculate the matching score between ROI images, where the structure of fingers is not always considered. On the other hand, the proposed algorithm normalizes the deformation between ROI images in consideration of the structure of fingers, and then calculates the matching score.

4. Experiments and discussion

This section describes a set of experiments using the PolyU FKP database [31] for evaluating the performance of the FKP recognition algorithms. First, we compare the three FKP recognition algorithms using the phase-based image matching described in Section 3: (A) the FKP recognition algorithm using BLPOC [11], (B) the FKP recognition algorithm using phase-based correspondence matching [34], and (C) the proposed algorithm. Then, we compare the performance of the proposed algorithm with the state-of-the-art conventional algorithms. Next, we consider the use of multiple FKP images to recognize a person using the PolyU FKP database.

The PolyU FKP database consists of 7920 images (384 × 288 pixels) with 165 subjects and 6 different images for each of the left index finger, the left middle finger, the right index finger and the right middle finger in 2 separate sessions. In the experiment, the images in the first session belong to the gallery set, while the images in the second session belong to the probe set, where each session consists of 660 (165 × 4) classes and 3960 (660 × 6) images. In the PolyU FKP database,

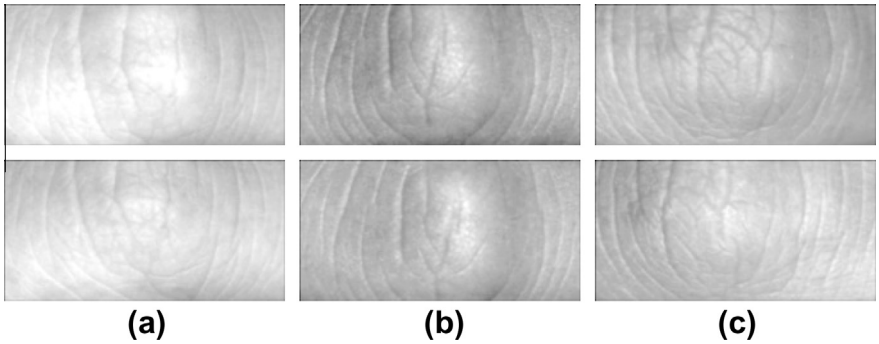

Fig. 4. Examples of FKP ROI images in the PolyU FKP database: FKP image pairs with different lighting condition (a) and nonlinear deformation (b) and (c).

ROI images extracted by the method proposed in Ref. [14] are also included, where the image size of ROI is 220 × 110 pixels. To compare the matching performance of the proposed method with the conventional methods reported in literature, we use the ROI images in the experiments. Fig. 4 shows some examples of FKP ROI images in this database. As shown in this figure, FKP images in the database are captured under different lighting condition and have rotation, translation and nonlinear distortion due to the movement of a finger.

4.1. Parameters for FKP recognition algorithms

This subsection describes the parameters for FKP recognition algorithms (A), (B) and (C) used in the experiments.

For the algorithm (A), we employ parameters for BLPOC as $K_1/M_1 = 0.25$ and $K_2/M_2 = 0.2$ which are optimized for PolyU FKP database in Ref. [17]. The algorithm (A) does not consider the large translational displacement between ROI images. Hence, we empirically determine that the threshold for the area ratio is 0.5.

In the algorithm (B), we employ the phase-based correspondence matching to obtain the corresponding point pairs and the local block matching using BLPOC to calculate the matching score. For the correspondence matching, we have to determine the parameters such as the number of layers l_{max} and the size of local block image W_c. The number of layers l_{max} is determined from the size of ROI images (220 × 110 pixels). In the experiments, we employ $l_{max} = 2$. The size of local block image W_c is optimized using all the genuine pairs (165 subjects × 4 classes × 6 images from 1st session × 6 images from 2nd session = 23,760 pairs) so as to maximize the 100th-lowest matching score. In the experiments, we employ $W_c = 48$. For the matching score calculation, we have to determine the size of local block image W and the parameters of BLPOC K_1/M_1 and K_2/M_2. In the experiments, we employ parameters as $W = 32$ and $K_1/M_1 = K_2/M_2 = 0.5$ which are the same in Ref. [34].

In the algorithm (C), we employ the phase-based correspondence matching for global and local registration. For the global registration, we have to determine the parameters such as the number of layers l_{max}, the size of local block image W_c and the threshold of local block similarity th. We employ $l_{max} = 2$ which can be determined from the size of ROI images. The size of local block images W_c and the threshold of local block similarity th are optimized using all the genuine pairs so as to maximize the 100th-lowest matching score as well as the algorithm (B). In the experiments, we employ $W_c = 48$ and $th = 0.29$. For the local registration and the matching score calculation, we have to determine the parameters such as the size of local block image W and the parameters for BLPOC K_1/M_1 and K_2/M_2. In the experiments, we employ the same parameters for the algorithm (B) such as $W = 32$ and $K_1/M_1 = K_2/M_2 = 0.5$. Note that the parameters for the proposed algorithm (C) is not so sensitive. For example, the recognition performance of the proposed algorithm (C) is comparable even for $th = 0.25$–0.33 and $W = 32$, 48.

4.2. Performance evaluation using single FKP image

The performance of the biometrics-based verification system is evaluated by the Receiver Operating Characteristic (ROC) curve, which illustrates the False Reject Rate (FRR) against the False Accept Rate (FAR) at different thresholds on the matching score. We first evaluate the FRR for all the possible combinations of genuine attempts; the number of attempts is 23,760. Next, we evaluate the FAR for all the possible combinations of imposter attempts; the number of attempts is 15,657,840. The performance is also evaluated by the Equal Error Rate (EER), which is defined as the error rate where the FRR and the FAR are equal.

Fig. 5 shows the ROC curves and EERs for each algorithm, and Fig. 6 shows the matching score distributions of genuine and imposter pairs for each algorithm. The EER of the algorithms (B) and (C) is significantly low compared with that of the

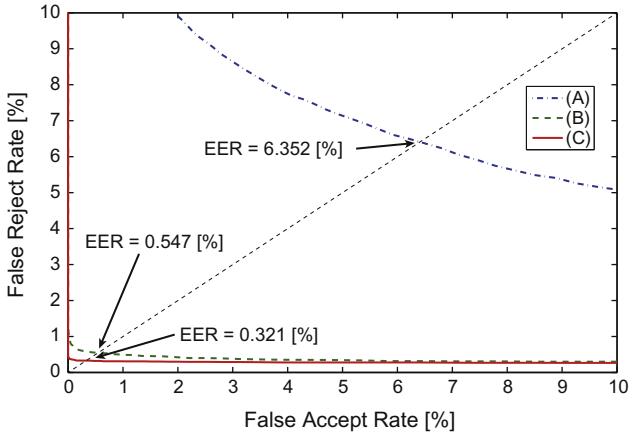

Fig. 5. ROC curves and EERs of the algorithms (A), (B) and (C).

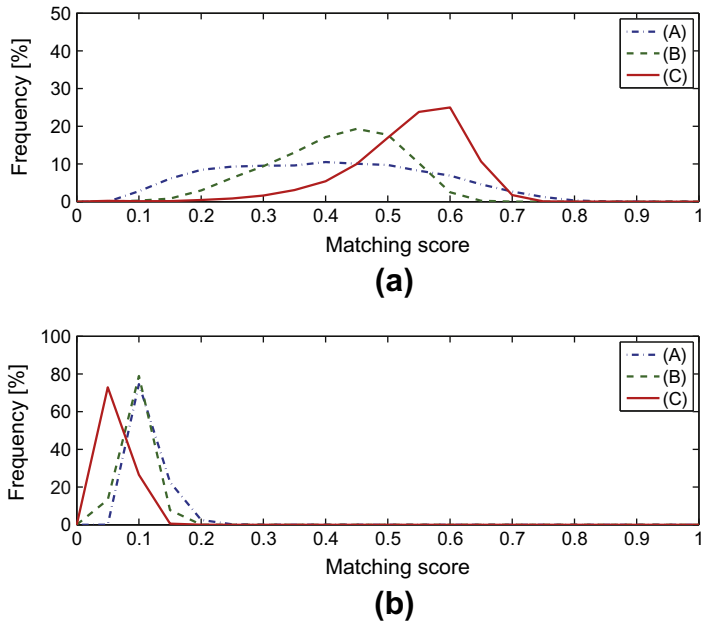

Fig. 6. Matching score distribution for algorithms (A), (B) and (C): (a) distribution of genuine pairs and (b) distribution of imposter pairs.

Table 2
EERs and d' of the FKP recognition algorithms.

Algorithm	EER [%]	d'
OE-SIFT [16]	0.850	–
CompCode [17]	1.658	4.2989
ImCompCode & MagCode [17]	1.475	4.3224
BLPOC [17]	1.676	2.4745
LGIC [17]	0.402	4.5356
$LGIC_2$ [18]	0.358	4.7001
(A) BLPOC	6.352	2.4529
(B) Correspondence matching	0.547	4.3905
(C) Proposed	**0.321**	**6.9424**

algorithm (A), since the algorithm (A) does not consider the deformation of FKP images. Comparing the algorithm (B) and (C), the matching score distribution of genuine pairs for the algorithm (C) is higher than that for the algorithm (B), and also the matching score distribution of imposter pairs for the algorithm (C) is lower than that for the algorithm (B). This fact indicates that the algorithm (C) is suitable for recognizing FKP images compared with the algorithm (B), since the algorithm (C) considers both global and local deformation of FKP images to calculate the matching scores between the FKP images.

Table 2 shows the EERs [%] and d' values of FKP recognition algorithms: OE-SIFT [16], CompCode [10], ImCompCode & MagCode [14], BLPOC [11], LGIC [17], $LGIC_2$ [18] and the proposed algorithm. d' is the index of how well the genuine and the imposter distributions are separated and is given by

$$d' = \frac{\sqrt{2}|\mu_{\text{genuine}} - \mu_{\text{imposter}}|}{\sqrt{\sigma^2_{\text{genuine}} + \sigma^2_{\text{imposter}}}}, \tag{15}$$

where μ_{genuine} and μ_{imposter} are the mean value of genuine and imposter matching scores, respectively, and σ_{genuine} and σ_{imposter} are the standard deviation of genuine and imposter matching scores, respectively. Note that EERs and d' for the conventional algorithms are referred from cited papers in Table 2, where the experimental conditions such as the number of genuine and imposter pairs are the same in all the algorithms. The EER of BLPOC is different between Ref. [11] and this paper, since the software implementations are different from each other. From Table 2, the proposed algorithm exhibits significantly good recognition performance compared with the state-of-the-art conventional FKP recognition algorithms.

Table 3 shows the computation time of each FKP recognition algorithm, where the evaluation environment for each algorithm is shown in Table 4. The computation time of the proposed algorithm is about 0.2 s. with MATLAB implementation, and

Table 3
Computation time of the FKP recognition algorithms.

Algorithm	Time
OE-SIFT [16]	<1 s
CompCode [17]	60.3 ms
ImCompCode & MagCode [14]	106.6 ms
BLPOC [17]	2.1 ms
LGIC [17]	63.8 ms
$LGIC_2$ [18]	408 ms
(A) BLPOC	5.9 ms
(B) Correspondence matching	200.8 ms
(C) Proposed	204.4 ms

Table 4
Evaluation environment for computation time of FKP recognition algorithms.

	Ref. [16]	Refs. [14,17,18]	Ours
CPU	Intel Pentium Dual-Core (1.66 GHz)	Intel Core 2 Duo E6550 (2.33 GHz)	Intel Xeon X5690 (3.46 GHz)
Implementation	–	Visual C#.Net 2005	MATLAB 7.14.0

Table 5
EERs and d' for each finger and multiple fingers, where ( ) indicates the EER and d' of the left index FKP images without one image pair shown in Fig. 7.

Finger	EER [%]	d'
Left index	0.683 (0.232)	6.5112 (6.9399)
Left middle	0.347	7.1631
Right index	0.082	6.8428
Right middle	0.175	5.9515
Index and middle	0.0078	8.6736

thus the computation time can be reduced by translating the MATLAB code to other implementation-oriented languages such as C/C++.

4.3. Performance evaluation using multiple FKP images

In the practical situation, the system can allow input of multiple FKP images such as index and middle fingers to recognize a person. It could result in improving the performance of the FKP recognition system.

First, we evaluate the performance for each finger. In this case, the number of genuine pairs is 5940 and the number of imposter pairs is 974,160 for each finger. Table 5 shows EERs and d' for each finger. Note that, in the left index FKP images, the matching score of one subject is significantly low, since there is a large movement of a finger between first and second sessions and also the images taken in the first session have a scab, while the images taken in the second session do not have it as shown in Fig. 7. Hence, we evaluate the performance of the left index FKP images without one subject shown in Fig. 7, and indicate the result values with the parenthesis in Table 5. From the experimental results, the EERs of right fingers are lower than those of the left fingers, while d' of all the fingers is almost the same.

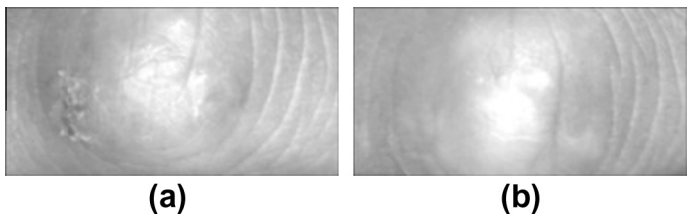

Fig. 7. A pair of left index FKP images which matching score is significantly low: (a) the image taken in the first session (/098_left index/01ROI.jpg) and (b) the image taken in the second session (/098_left index/07ROI.jpg).

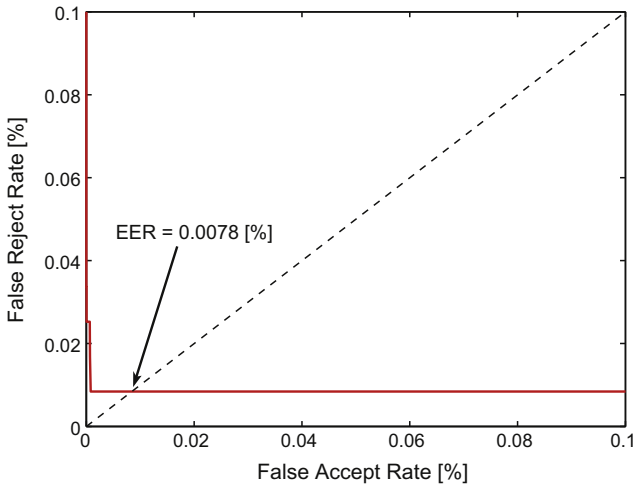

Fig. 8. ROC curve for the use of multiple fingers (index and middle fingers).

To evaluate the performance of the use of multiple FKP images in the PolyU FKP database, we consider the situation that a person inputs the FKP images taken from the index and middle fingers of a hand, where we assume that the left and right hands are taken from different persons. In other words, we evaluate the performance using FKP images taken from the index and middle fingers of 330 subjects. In this case, the number of genuine pairs is 11,880 and the number of imposter pairs is 3,908,520. The matching score S for multiple FKP images is defined by

$$S = \frac{S_{\text{index}} + S_{\text{middle}}}{2}, \tag{16}$$

where S_{index} and S_{middle} indicate the matching score for index and middle fingers, respectively. Fig. 8 shows the ROC curve for the use of multiple fingers, and the bottom row in Table 5 shows the EER and d'. As a result, the EER for the use of multiple fingers is significantly low compared with that for the use of a single finger. Thus, we can enhance the recognition performance of the FKP recognition algorithm by using multiple fingers.

5. Conclusion

This paper has proposed an FKP recognition algorithm using BLPOC-based local block matching. The proposed algorithm employs the global and local registration of FKP images to obtain the reliable matching score. The experiments using the PolyU FKP database demonstrate that the proposed algorithm exhibits higher recognition performance than the state-of-the-art conventional algorithms. In addition, we demonstrate that the use of multiple fingers makes it possible to significantly improve the performance of the FKP recognition algorithm. In the future, we will develop the practical FKP recognition system with multiple finger acquisition.

References

[1] A. Jain, P. Flynn, A. Ross, Handbook of Biometrics, Springer, 2008.
[2] D. Maltoni, D. Maio, A.K. Jain, S. Prabhakar, Handbook of Fingerprint Recognition, Springer, 2003.
[3] D. Zhang, Palmprint Authentication, Kluwer Academic Publication, 2004.
[4] A. Kong, D. Zhang, M. Kamel, A survey of palmprint recognition, Pattern Recognition 42 (7) (2009) 1408–1418.
[5] H. Li, J. Zhang, Z. Zhang, Generating cancelable palmprint templates via coupled nonlinear dynamic filters and multiple orientation palmcodes, Information Sciences 180 (20) (2010) 3876–3893.
[6] D. Zhang, W. Zuo, F. Yue, A comparative study of palmprint recognition algorithms, ACM Computing Surveys 44 (1) (2012) 2:1–2:37.
[7] N. Duta, A survey of biometric technology based on hand shape, Pattern Recognition 42 (2009) 2797–2806.
[8] D. Woodard, P. Flynn, Finger surface as a biometric identifier, Computer Vision and Image Understanding 100 (2005) 357–384.
[9] M. Ferrer, C. Travieso, J. Alonso, Using hand knuckle texture for biometric identifications, IEEE Aerospace and Electronic Systems Magazine 21 (6) (2006) 23–27.
[10] L. Zhang, L. Zhang, D. Zhang, Finger-knuckle-print: a new biometric identifier, in: Proc. Int'l Conf. Image Processing, 2009, pp. 1981–1984.
[11] L. Zhang, L. Zhang, D. Zhang, Finger-knuckle-print verification based on band-limited phase-only correlation, Lecture Notes in Computer Science 5702 (2009) 141–148.
[12] A. Kumar, Y. Zhou, Human identification using knucklecodes, in: Proc. Int'l Conf. Biometrics: Theory, Applications and Systems, 2009, pp. 1–6.
[13] A. Kumar, C. Ravikanth, Personal authentication using finger knuckle surface, IEEE Transactions on Information Forensics and Security 4 (1) (2009) 98–110.
[14] L. Zhang, L. Zhang, D. Zhang, H. Zhu, Online finger-knuckle-print verification for personal authentication, Pattern Recognition 43 (2010) 2560–2571.
[15] M. Xiong, W. Yang, C. Sun, Finger-knuckle-print recognition using LGBP, in: Proc. Int'l Conf. Advances in Neural Networks Part II, 2011, pp. 270–277.
[16] A. Morales, C. Travieso, M. Ferrer, J. Alonso, Improved finger-knuckle-print authentication based on orientation enhancement, IEEE Electronics Letters 47 (6) (2011) 380–381.

[17] L. Zhang, L. Zhang, D. Zhang, H. Zhu, Ensemble of local and global information for finger-knuckle-print recognition, Pattern Recognition 44 (2011) 1990–1998.
[18] L. Zhang, L. Zhang, D. Zhang, Z. Guo, Phase congruency induced local features for finger-knuckle-print recognition, Pattern Recognition 45 (2012) 2522–2531.
[19] L. Zichao, K. Wang, W. Zuo, Finger-knuckle-print recognition using local orientation feature based on steerable filter, in: Proc. Int'l Conf. Intelligent Computing, vol. 304, 2012, pp. 224–230.
[20] A. Kumar, Can we use minor finger knuckle images to identify humans? in: Proc. Int'l Conf. Biometrics: Theory, Applications and Systems, 2012, pp. 55–60.
[21] N. Mittal, M. Hanmandlu, R. Vijay, A finger-knuckle-print authentication system based on DAISY descriptor, in: Proc. Int'l Conf. Intelligent Systems Design and Applications, 2012, pp. 126–130.
[22] L. Zhang, H. Li, Encoding local image patterns using Riesz transforms: with applications to palmprint and finger-knuckle-print recognition, Image and Vision Computing (2012) 1043–1051.
[23] G. Michael, T. Connie, A. Jin, An innovative contactless palm print and knuckle print recognition system, Pattern Recognition Letters 31 (2010) 1708–1719.
[24] L. Zhu, S. Zhang, Multimodal biometric identification system based on finger geometry, knuckle print and palm print, Pattern Recognition Letters 31 (2010) 1641–1649.
[25] E. Tola, V. Lepetit, P. Fua, DAISY: an efficient dense descriptor applied to wide baseline stereo, IEEE Transactions on Pattern Analysis and Machine Intelligence 32 (5) (2010) 815–830.
[26] C.D. Kuglin, D.C. Hines, The phase correlation image alignment method, in: Proc. Int'l Conf. Cybernetics and Society, 1975, pp. 163–165.
[27] K. Takita, T. Aoki, Y. Sasaki, T. Higuchi, K. Kobayashi, High-accuracy subpixel image registration based on phase-only correlation, IEICE Transactions on Fundamentals E86-A (8) (2003) 1925–1934.
[28] K. Ito, H. Nakajima, K. Kobayashi, T. Aoki, T. Higuchi, A fingerprint matching algorithm using phase-only correlation, IEICE Transactions on Fundamentals E87-A (3) (2004) 682–691.
[29] K. Ito, T. Aoki, H. Nakajima, K. Kobayashi, T. Higuchi, A palmprint recognition algorithm using phase-only correlation, IEICE Transactions on Fundamentals E91-A (4) (2008) 1023–1030.
[30] K. Miyazawa, K. Ito, T. Aoki, K. Kobayashi, H. Nakajima, An effective approach for iris recognition using phase-based image matching, IEEE Transactions on Pattern Analysis and Machine Intelligence 30 (10) (2008) 1741–1756.
[31] PolyU FKP Database. <http://www4.comp.polyu.edu.hk/biometrics/FKP.htm>.
[32] A. Oppenheim, R. Schafer, J. Buck, Discrete-Time Signal Processing, second ed., Prentice Hall, 1999.
[33] K. Takita, M.A. Muquit, T. Aoki, T. Higuchi, A sub-pixel correspondence search technique for computer vision applications, IEICE Transactions on Fundamentals E87-A (8) (2004) 1913–1923.
[34] K. Ito, S. Iitsuka, T. Aoki, A palmprint recognition algorithm using phase-based correspondence matching, in: Proc. Int'l Conf. Image Processing, 2009, pp. 1977–1980.